Since January 2020 Elsevier has created a COVID-19 resource centre with free information in English and Mandarin on the novel coronavirus COVID-19. The COVID-19 resource centre is hosted on Elsevier Connect, the company's public news and information website.

Antiviral Research 193 (2021) 105138

Contents lists available at ScienceDirect

Antiviral Research

journal homepage: www.elsevier.com/locate/antiviral

A mouse model of lethal respiratory dysfunction for SARS-CoV-2 infection

Esther S. Gan [a,**], Ayesa Syenina [a,b], Martin Linster [a], Benson Ng [c], Summer L. Zhang [a], Satoru Watanabe [a], Ravisankar Rajarethinam [d], Hwee Cheng Tan [a], Gavin JD. Smith [a], Eng Eong Ooi [a,b,e,*]

[a] Program in Emerging Infectious Diseases, Duke-NUS Medical School, 8 College Road, Singapore, 169857, Singapore
[b] Viral Research and Experimental Medicine Centre, SingHealth Duke-NUS Academic Medical Centre, 20 College Road, Singapore, 169856, Singapore
[c] Office of Research Affairs, Duke-NUS Medical School, 8 College Road, Singapore, 169857, Singapore
[d] Institute of Molecular and Cell Biology (IMCB), Agency for Science, Technology and Research (A*STAR), 61 Biopolis Drive, Singapore, 138673, Singapore
[e] Saw Swee Hock School of Public Health, National University of Singapore, 12 Science Drive 2, #10-01, Singapore, 117549, Singapore

ARTICLE INFO

Keywords:
SARS-CoV-2
K18-hACE2 mice
Genetic variants
Pneumonia

ABSTRACT

The global spread of SARS-CoV-2 has made millions ill with COVID-19 and even more from the economic fallout of this pandemic. Our quest to test new therapeutics and vaccines require small animal models that replicate disease phenotypes seen in COVID-19 cases. Rodent models of SARS-CoV-2 infection thus far have shown mild to moderate pulmonary disease; mortality, if any, has been associated with prominent signs of central nervous system (CNS) infection and dysfunction. Here we describe the isolation of SARS-CoV-2 variants with propensity for either pulmonary or CNS infection. Using a wild-type SARS-CoV-2 isolated from a COVID-19 patient, we first found that infection was lethal in transgenic mice expressing the human angiotensin I-converting enzyme 2 (hACE2). Fortuitously, full genome sequencing of SARS-CoV-2 from the brain and lung of these animals showed genetic differences. Likewise, SARS-CoV-2 isolates from brains and lungs of these also showed differences in plaque morphology. Inoculation of these brain and lung SARS-CoV-2 isolates into new batch of hACE2 mice intra-nasally resulted in lethal CNS and pulmonary infection, respectively. Collectively, our study suggests that genetic variants of SARS-CoV-2 could be used to replicate specific features of COVID-19 for the testing of potential vaccines or therapeutics.

1. Introduction

The severe acute respiratory syndrome coronavirus-2 (SARS-CoV-2), which emerged at the end of 2019 in China, has spread throughout the world to cause the coronavirus disease-19 (COVID-19) pandemic. Millions have developed COVID-19 and ~2.5% of whom have died from respiratory dysfunction (L. Wang et al., 2020b). Some have also developed severe systemic complications, such as coagulopathy (Zhou et al., 2020). Vaccine development has made unprecedented progress (Krammer, 2020) although the durability of immunity afforded by the front-running vaccines remain unknown. With a handful of exceptions, most therapeutics against SARS-CoV-2 and COVID-19 have not shown useful efficacy in improving disease outcome in clinical trials (Kaddoura et al., 2020). The availability of a small animal model that reproducibly manifests important clinical features of COVID-19 could be instrumental in supporting the development of improved therapeutics and even vaccines.

SARS-CoV-2 is unable to engage mouse ACE2 as a receptor for infection (Wan et al., 2020). Transgenic mice expressing the human ACE2 receptor have thus been used to develop a SARS-CoV-2 infection model. Until recently, SARS-CoV-2 infection in such mice was shown to produce detectable infection and associated histopathological changes but without reproducible mortality (Bao et al., 2020; Golden et al., 2020; Israelow et al., 2020; Jiang et al., 2020; Winkler et al., 2020). A recent study reported 100% mortality in SARS-CoV-2 infected K18 hACE2 mice (Golden et al., 2020). The K18-hACE2 transgenic mice expresses the human ACE2 protein under the control of the epithelial cell cytokeratin (K18) promoter (Chow et al., 1997). The expression of hACE2 has been found not only in epithelial cells lining the respiratory tract, but also in the kidney, liver, spleen and small intestine of these animals. It is also

* Corresponding author. Program in Emerging Infectious Diseases, Duke-NUS Medical School, 8 College Road, Singapore, 169857, Singapore.
** Corresponding author.
E-mail addresses: esther.gan@duke-nus.edu.sg (E.S. Gan), engeong.ooi@duke-nus.edu.sg (E.E. Ooi).

https://doi.org/10.1016/j.antiviral.2021.105138
Received 15 June 2021; Received in revised form 4 July 2021; Accepted 7 July 2021
Available online 8 July 2021

expressed at low levels in the brain of these animals(McCray et al., 2007a,b). Thus, while these animals succumbed to SARS-CoV-2 infection, clinical signs that led to eventual mortality were due mostly to the central nervous system (CNS) dysfunction. Moreover, high SARS-CoV-2 burden was also found in the brains of these animals. Thus, while COVID-19 is primarily a pulmonary disease in humans, lethal mouse models of SARS-CoV-2 infection is mostly due to CNS complications.

Herein, we describe an unexpected finding of SARS-CoV-2 mutations in K18-hACE2 mice that produces specificity in either CNS or respiratory dysfunction. While we had set out to establish a SARS-CoV-2 infection model in this strain of transgenic mice, we serendipitously recovered genetic variants of SARS-CoV-2 that produce lethal pulmonary or CNS infection, respectively. Full genome sequencing revealed mutations in the S1–S2 boundary of the spike (S) protein in viruses isolated from the brain; intra-nasal inoculation of this brain-derived SARS-CoV-2 isolate into susceptible mice reproduced mortality from CNS dysfunction. In contrast, the SARS-CoV-2 isolated from the lung of K-18 hACE2 mice lacked these mutations; re-infection with this isolate via the intra-nasal route produced respiratory dysfunction exclusively. A small animal model that reproduces features of acute respiratory dysfunction upon SARS-CoV-2 infection could be particularly useful in pre-clinical evaluation of respiratory agents as treatment for severe COVID-19.

2. Material and methods

2.1. Study approvals

All mouse studies were performed in accordance to protocols approved by the Institutional Animal Care and Use Committee at Singapore Health Services, Singapore (ref no.: 2020/SHS/1554).

2.2. Ethics statement

All studies were performed in accordance with guidelines provided by the National Advisory Committee for Laboratory Animal Research (NACLAR) in Singapore. All protocols in this study has been approved by the Institutional Animal Care and Use Committee at Singapore Health Services (Protocol #2020/SHS/1554).

2.3. Animal studies

All studies conducted in this studies utilized female B6; SJL-Tg(K18-hACE2)2Prlmn/J (K18-hACE2) mice purchased from Jackson laboratory were housed in a BSL-2 animal facility at Duke-NUS Medical School. Groups of 6–8 weeks old K18-hACE2 female mice (n = 5) were infected with Sars-CoV-2 Strain SG12 (GISAID accession code EPI_ISL_406973) at 2×10^5 or 2×10^4 PFU in 50 μl via the intranasal route at the Duke-NUS Medical School animal biosafety level 3 laboratory. Daily weight measurements and clinical scores were obtained. Mice were sacrificed when exhibiting greater than 20% weight loss or reaching a clinical score of 10 (Supplementary Table 1). To assess organ viral loads, mice were sacrificed 5 days post infection and harvested organs were frozen at −80 °C. Organs were homogenized in MP lysing matrix A and F according to manufacturer's instructions in 1 ml PBS. Homogenates were used to perform plaque assays.

2.4. RNA extraction

RNA was then extracted from the homogenate using a TRIzol LS (ThermoFisher #10296010) and chloroform method to induce phase separation. Organ RNA concentration was measured using the NanoDrop 2000 Spectrophotometer (Thermo- Fisher).

2.5. Plaque assay and plaque size quantification

Organ homogenates were serially diluted in culture media, added to Vero-E6 cells (ATCC) in 24 well plates. Cultures were then incubated for 1hr at 37 °C and overlayed with carboxymethyl cellulose (CMC) and incubated at 37 °C, 5% CO_2. Five days later, cells were washed, stained with 1% crystal violet and plaques counted. Plaque sizes were measured in pixel density using ImageJ.

2.6. Virus propagation

Organ homogenates were diluted in culture media, added to Vero-E6 at a MOI of 0.01.3 days later, culture supernatant were centrifuged to remove cellular debris and stored at −80 °C.

2.7. Histology

Mice lungs were inflated and fixed in 10% neutral buffered formalin for about 72 h at room temperature. They were routinely processed and then embedded in paraffin blocks. Tissues were sectioned at 5 μm thickness, and stained with Hematoxylin and Eosin (H&E). Histopathological assessment was performed in a blind fashion using Olympus BX53 upright microscope and representative photomicrographs were captured with an Olympus DP71 digital colour camera with Olympus DP controller and DP manager software (Olympus Life Science, Japan). Presence of lesions was scored according to previously published criteria (Shackelford et al., 2002).

2.8. SARS-CoV-2 genome sequencing

SARS-CoV-2 RNA from lung and brain homogenates were sequenced using an amplicon-based framework (https://www.protocols.io/view/ncov-2019-sequencing-protocol-v3-locost-bh42j8ye). Briefly, cDNA was synthesized from RNA extracted from lung and brain tissues using the SuperScript IV First-Strand Synthesis System (Life Technologies) with random hexamers. Amplicons were then generated using Q5 Hot Start High-Fidelity DNA Polymerase (New England Biolabs) with the ARTIC network primer scheme V3 (https://artic.network/ncov-2019). The PCR mixture was initially incubated for 30s at 98 °C for denaturation, followed by 25 cycles of 98 °C for 15 s and 65 °C for 5 min. The PCR products were then diluted 10-fold. Subsequently, the diluted amplicons were end-prepped and dA-tailed using NEBNext Ultra II End Repair/dA-Tailing Module. Native barcodes and sequencing adapters supplied in the EXP-NBD101/114 kit (Oxford Nanopore Technologies) were attached to the dA-tailed amplicons using NEB Blunt/TA Ligase 2x Master Mix and NEBNext Quick Ligation Kit, respectively. Finally, 15 ng of DNA library was loaded on to the R9.4.1 flow cell following the SQK-LSK109 ligation sequencing kit (Oxford Nanopore Technologies) protocol, the sequencing run was performed for a total of 6 h. Reads were determined using the MinKnow software with the high-accuracy base-calling algorithm.

Sequence analysis was conducted using the ARTIC network ncov2019 bioinformatics pipeline (https://artic.network/ncov-2019). Briefly, demultiplexing and primer/quality trimming of reads were performed using Guppy. In order to remove chimeric reads, reads were filtered to stretches of a minimum length of 400bp and maximum length of 700. After trimming, reads were mapped to hCoV-19/Singapore/2/2020|EPI_ISL_407987|2020-01-25 using Minimap2. Finally, SNV analysis was carried out using Geneious Prime® 2020.2.4.

2.9. Nanostring

100 ng of extracted RNA from lung and brain homogenates were hybridized to the Nanostring nCounter mouse inflammation panel at 65 °C for 24 h. Hybridized samples were quantified using the nCounter Sprint profiler. Data was analyzed using the nSolver Analysis Software (NanoString Technologies). Subsequent pathway analysis was performed using EnrichR (https://maayanlab.cloud/Enrichr/).

2.10. Statistics

All in vivo experiments were performed with 5 animals per group. A 2-tailed unpaired T test was performed to compare between the means of two conditions using Graphpad Prism (v8). The Kaplan-Meier (log rank) test was used to compare 2 survival curves using Graphpad Prism. For all data sets, a p value of less than 0.05 was considered significant.

3. Results

3.1. SARS-CoV-2 infection results in severe and fatal infections of K18-hACE2 mice

To determine the clinical outcome of SARS-CoV-2 infection in K18-hACE2 mice, two groups of mice aged 6–8 weeks (n = 4 per group) were intranasally inoculated with 2×10^5 (high dose) or 2×10^4 PFU (low dose) of SARS-CoV-2 (SG12) (hCoV-19/Singapore/2/2020); the full genome sequence of SG12 has been previously reported in GSAID (EPI_ISL_407987) (Su et al., 2020). All animals were observed daily for weight loss and other clinical signs for 8 days (Fig. 1A). Two out of four (50%) animals inoculated with low-dose but not high-dose SARS-CoV-2 showed weight loss from 3 days post infection (dpi) onwards. At 4 dpi, both groups of infected K18-hACE2 mice exhibited lethargy and weight loss, with the exception of one animal inoculated with low-dose SARS CoV-2 (Fig. 1B). Signs of CNS dysfunction, such as tremor and non-responsiveness to stimuli (Fig. 1C), as well as respiratory distress (labored breathing) (Fig. 1D) and were evident at 3 and 5 dpi, respectively, in both groups of infected animals. CNS signs such as abnormal gait, shaking and paralysis were, however, predominant (Supplementary Table 1). The total clinical scores thus mostly reflected CNS dysfunction. Three out of four (75%) animals inoculated with low-dose SARS-CoV-2 met euthanasia criteria (clinical scores above 10) and were thus sacrificed between 5 and 7 dpi (Fig. 1E and F). No statistical significance in survival was observed between low and high dose challenge suggesting that infection with 2×10^4 PFU was sufficient for a lethal infection.

3.2. SARS-CoV-2 infection produces clinically compatible pulmonary histopathological features in K18-hACE2 mice

Although infected mice died mostly of CNS dysfunction, we nonetheless asked if SARS-CoV-2 infection in these animals produced pulmonary pathology consistent with those found in fatal COVID-19 cases. We carried out histopathological investigations on formalin-fixed lungs of K18-hACE2 mice at 5 dpi, which was immediately before the onset of clinical signs that heralded mortality. Infection with both low- and high-dose SARS-CoV-2 produced multifocal to coalescing interstitial pneumonia in the lung parenchyma (Fig. 2A). The alveoli were collapsed with thickened and congested septa (Fig. 2B). Infiltration of mononuclear cells such as lymphocytes, macrophages and plasma cells were mainly

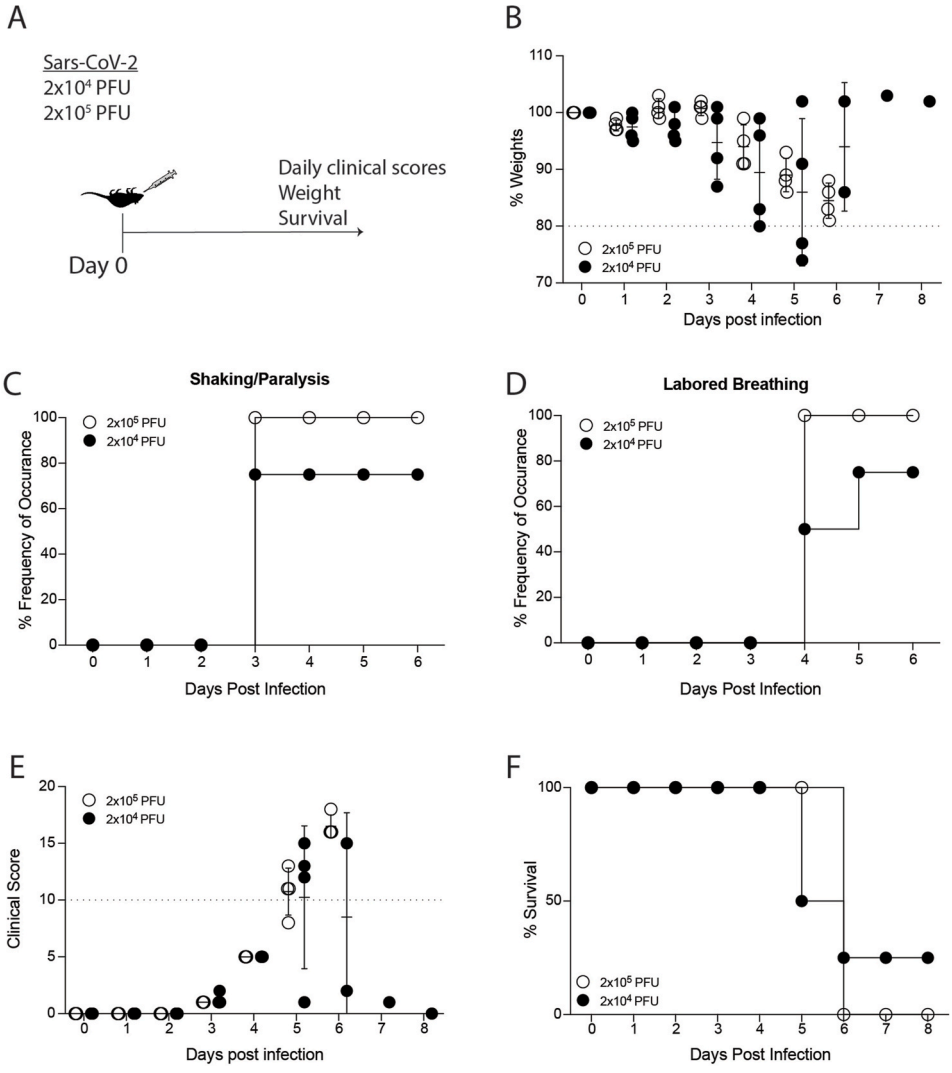

Fig. 1. SARS-CoV-2 infection in K18-hACE2 transgenic mice results in a lethal infection. (A) Experimental schematic of K18-hACE2 transgenic mice infection. (B) Combined weights of K18-hACE2 post SARS-CoV-2 infection. (C–D) Clinical scores indicating CNS (C) respiratory disease (D) of SG12-B and SG12-L infected K18-hACE2 mice post infection. (E–F) Weights (E) and survival (F) of K18-hACE2 post SARS-CoV-2 infection. Dashed line in 1B and C indicates the limit at which animals will be euthanized.

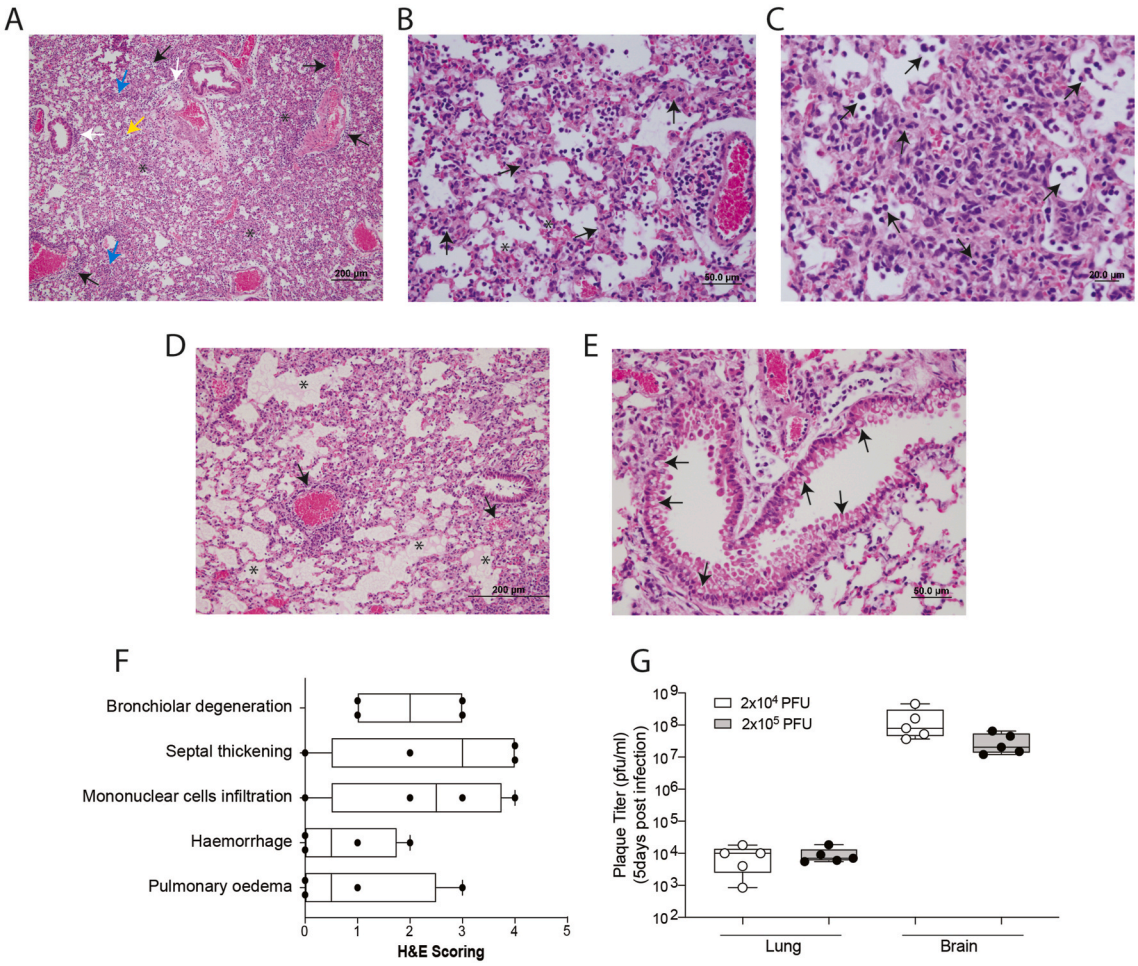

Fig. 2. SARS-CoV-2 infection in K18-hACE2 mice resulted in pulmonary pathology.
(A-E) Representative images of histopathological analysis 5 days post infection in K18-hACE2 mice inoculated with 2×10^4 PFU revealed interstitial pneumonia as represented by collapsed alveoli (asterisk) and multifocal inflammation in perivascular (black arrows), peribronchiolar (white arrows), septa (blue arrows) and alveolar sacs (yellow arrow) (A), alveolar septal thickening (arrow) and congestion (asterisk) (B), mononuclear cells infiltration (arrow) in alveolar parenchyma (C) pulmonary oedema (asterisk) displays pink stained homogenous materials that widens the interstitial area and perivascular infiltration (arrow) (D) and bronchiole vacuolar degeneration marked by cytoplasmic vacuolization (arrow) (E). (F) Semi quantitative analysis of histopathological findings is based on subjective scoring. 0-Nil, 1-Minimum, 2-Mild, 3-Moderate, 4-Marked, 5-Severe. (G) Viral loads in the lungs and brains of infected mice 5 days post infection as measured by plaque assay. (For interpretation of the references to colour in this figure legend, the reader is referred to the Web version of this article.)

observed at peri-vascular, peri-bronchioles, alveolar septa and alveolar sacs (Fig. 2C). Mild degree of pulmonary oedema (Fig. 2D) and occasional focal presence of haemorrhages were present. Minimal focal necrosis of alveoli was also observed. Vacuolar degeneration of lining epithelium was common from bronchus to terminal bronchioles (Fig. 2E). A semi-quantitative analysis of all four SARS-CoV-2 infected animal lungs suggest that bronchiolar degeneration, septal thickening and mononuclear cell infiltration are common virus induced pathological changes in K18-hACE2 mice (Fig. 2F). These findings are thus similar to previous observations on K18-hACE2 mouse model (Oladunni et al., 2020; Yinda et al., 2021), nonhuman primate infection model and deceased COVID-19 patients(Rockx et al., 2020; C. Wang et al., 2020a).

3.3. Infectious SARS-CoV-2 re-isolated from the lung and brain of K18-hACE2 mice

We next examined the sites of infection in various organs of SARS-CoV-2 infected female K18-hACE2 mice at 5 dpi. The brain, lung, eyes, spleen, liver and kidneys were dissected from infected animals and homogenized; clarified homogenates were then inoculated onto Vero-E6 cells. Cytopathic effects were observed in cells inoculated with lung and brain homogenates, but not those from the other organs (Supplementary Fig. 1). To define the viral burden in the lungs and brains at post mortem examination, we used plaque assay to quantify SARS-CoV-2 infectious particles in the lung and brain homogenates. SARS-CoV-2 plaque titers in the brain homogenates were approximately 4 logs higher than those in the lung (Fig. 2G). Moreover, the plaque morphology of the brain SARS-CoV-2 isolates (SG12-B) were punctate in size, which was in contrast to the extensive areas of plaques formed from the lung-derived isolates (SG12-L) (Supplementary Fig. 2A).

3.4. Genomic differences in SARS-CoV-2 isolates from lung and brain homogenates

Differences in the plaque morphology of the brain and lung isolates suggest viral adaptations during the course of infection that may be important for system-specific dysfunction. To test this possibility, we conducted full genome sequencing of SARS-CoV-2 RNA extracted from brain and lung homogenates, without isolation in cell lines, and compared these with the sequence of the SG12 virus – propagated in Vero E6 cells – that was inoculated into these animals. Compared to the original SG12 sequence, the virus we used for our infection study had 2 mutations in the ORF1ab, one consensus change – deletion at nucleotide position 517 to 519 (an ATG methionine deletion – M173del) (Fig. 3A

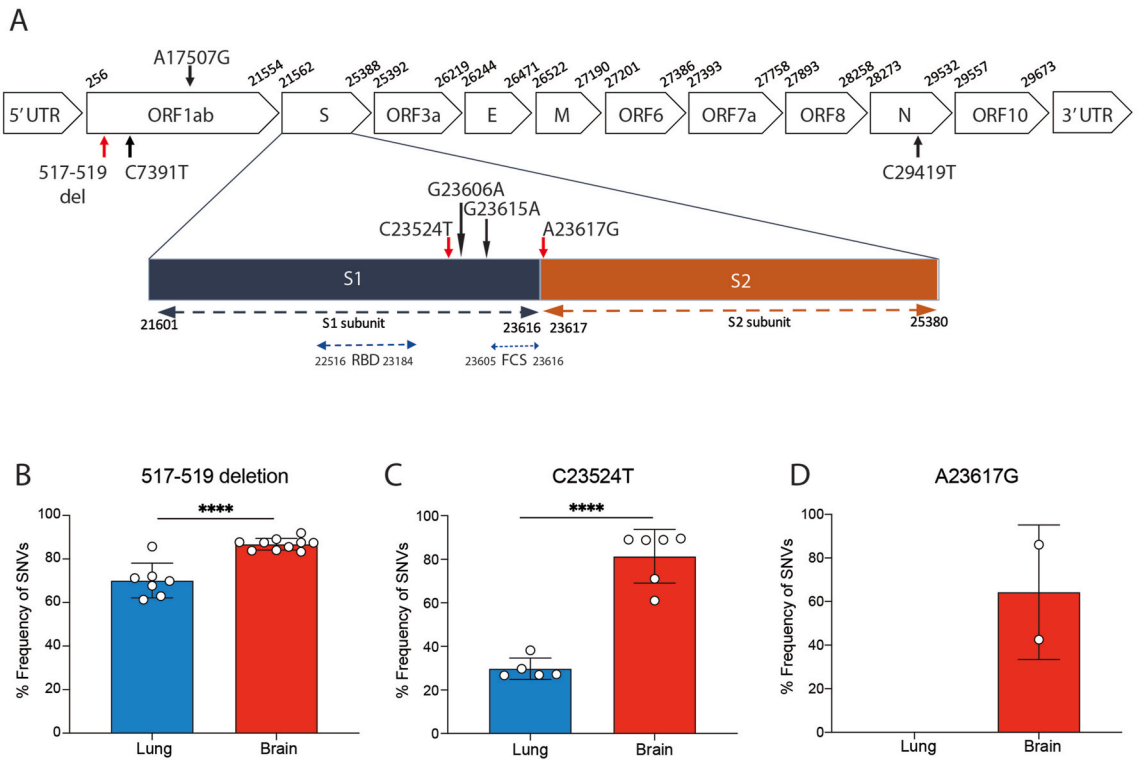

Fig. 3. Genetic differences in SARS-CoV-2 isolated from the brain and lungs of infected K18-hACE2 mice.
(A) SNVs mapped to its position in the SARS-CoV-2 genome. Red arrows depict consensus mutations and black arrows depicts non-consensus mutations. (B) SNV frequency of ATG deletion at nucleotide positions 517–519 in lung and brain samples (C) SNV frequency of C to T nucleotide substitution at position 23524 (H655Y) in lung and brain samples. (D) SNV frequency of A to G nucleotide substitution at position 23617 (S686G) in lung and brain samples. (For interpretation of the references to colour in this figure legend, the reader is referred to the Web version of this article.)

and B) and a C7391T substitution (amino acid substitution P2379L). These mutations were also present in both brain and lung samples (Fig. 3A).

Viruses isolated from the brain showed two consensus changes in the S gene - C23524T nucleotide substitution that corresponded to substitution of histidine with tyrosine (H655Y) (Fig. 3A and C) and A23617G nucleotide substitution that substituted serine with glycine (S686G) (Fig. 3A and D). While A23617G was found exclusively in the brain, C23524T was also found in the lung but as a non-consensus mutation (Fig. 3A, Supplementary Fig. 2B). Interestingly, A23617G and C23524T appeared to be mutually exclusive in brain samples: C23524T was observed in 6 out of 10 brain isolates, while A23617G were found in the remaining 4 animals. However, out of all the mutations observed, only C23524T could be mapped to the surface of the S1–S2 interface of the S protein (Supplementary Fig. 3), while structural information is not yet available for the other mutation. Besides the consensus mutations, non-consensus mutations were also detected in a minority of animals (Supplementary Fig. 2B). Collectively, these findings suggest viral factors could play important roles in the fate of infection in these animals.

3.5. Lung and brain isolates result in differing clinical outcomes

To test if the genetic differences between the brain and lung isolates of SARS-CoV-2 influenced system-specific dysfunction, we isolated SARS-CoV-2 from these organs in Vero E6 cells and used them to infect new batches of female mice. Brain- (SG12-B) and lung-derived (SG12-L) viruses (Fig. 4A) were selected using convenient sampling and were used to inoculate K18-ACE2 mice intra-nasally at a dose of 2×10^4 PFU (Fig. 4A). Mice were monitored daily for clinical scores and weight loss over a course of 7 days (Fig. 4A). Both SG12-B and SG12-L infected mice showed weight loss at 4 to 6 dpi (Fig. 4B). Mice infected with SG12-B succumbed to infection sooner than those infected with SG12-L ($P =$ 0.0311) (Fig. 4C). Strikingly, signs leading to euthanasia were different. All animals infected with SG12-B showed tremor and paralysis at 5 dpi; only 20% of animals infected with SG12-L displayed such signs (Fig. 4D). Conversely, SG12-L infected mice displayed labored breathing starting at 6 dpi (Fig. 4E); none of the SG12-B infected mice showed such sign of respiratory distress. Notably, while no difference in viral load was found in the lung of SG12-L and SG12-B infected animals (Fig. 4F), viral load in the brain was significantly higher in SG12-B than SG12-L infected animals (Fig. 4G). Moreover, the plaque morphology of SARS-CoV-2 isolated from SG12-B infected lungs were uniformly punctate and significantly smaller compared to those recovered from the lungs of SG12-L infected mice (Fig. 4H). In addition, further sequencing of viruses isolated from the lungs of SG12-L infected mice revealed identical sequence changes (517-519del and C23524T), suggesting that SG12-L is genetically stable.

The presence of both SG12-L and SG12-B in both lung and brain tissues indicates that the observed mutations were unlikely to determine tissue tropism. Instead, these mutations could contribute to differential host responses. As hyperinflammation has been associated with severe COVID-19, we measured the RNA transcripts of inflammatory genes in the lungs and brains of SG12-L and SG12-B infected animals using a previously defined inflammation panel from Nanostring technologies. Interestingly, despite comparable lung viral loads (Fig. 4F), inflammatory signatures identified from the lungs of SG12-L and SG12-B infected animals clustered separately on a PCA plot (Fig. 5A). Pathway analysis of the top 20 most correlated genes in PC1 that separated these gene clusters unsurprisingly identified pathways in pathogen and inflammatory responses, specifically chemokine signaling and cytokine-cytokine receptor interaction (Fig. 5B). Strikingly, lungs of SG12-L infected animals showed increased expression of inflammatory genes in both the chemokine signaling pathway (Fig. 5C) and cytokine-cytokine receptor signaling pathway (Fig. 5D). SG12-L also showed increased expression

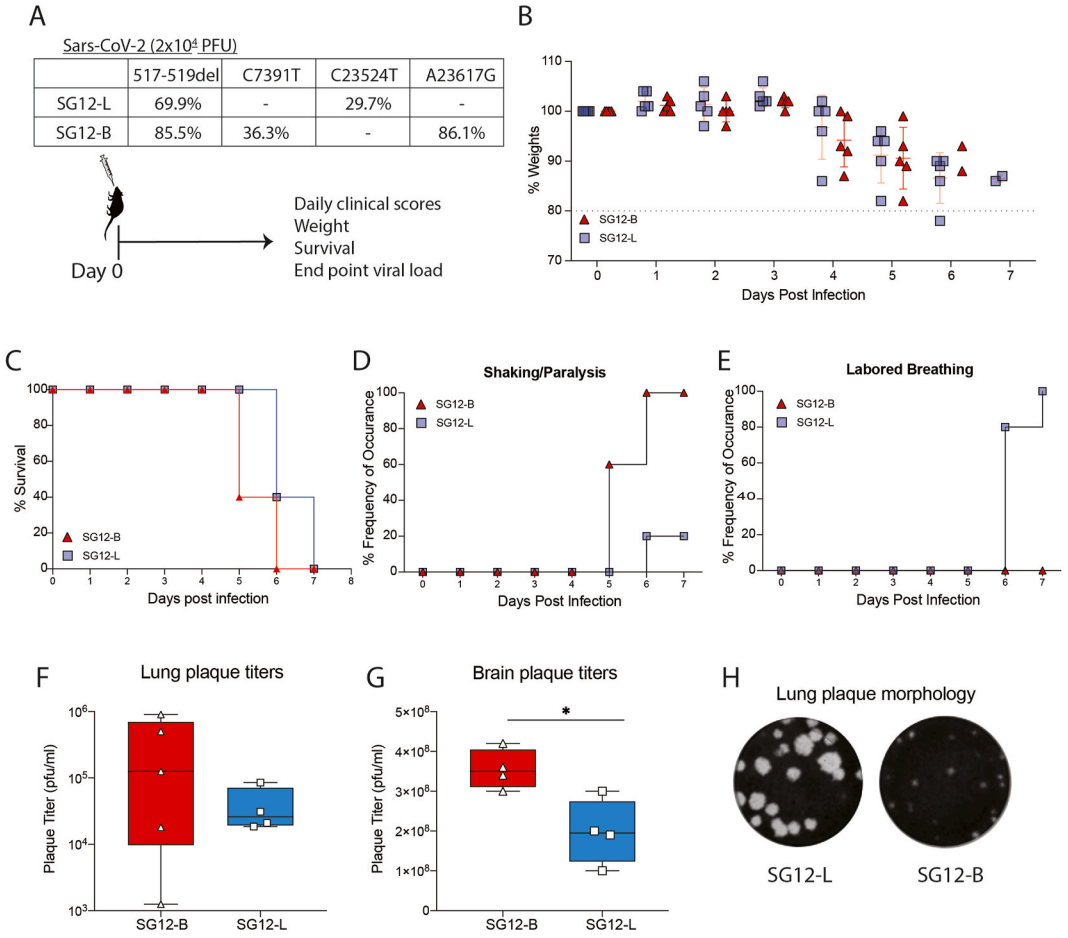

Fig. 4. SG12-B and SG12-L infection caused different clinical outcome

(A) Experimental schematic of K18-hACE2 transgenic mice infection with SG12-B and SG12-L. (B–C) Weight (B) and survival (C) of SG12-B and SG12-L infected K18-hACE2 mice post infection. (D–E) Clinical scores indicating respiratory (D) and CNS disease (E) of SG12-B and SG12-L infected K18-hACE2 mice post infection. (F–G) Viral loads of lung (F) and brains (G) of K18-hACE2 mice infected with SG12-B and SG12-L upon euthanasia measured by plaque assay. (H) Representative images of lung plaque morphology from animals infected with SD12-L and SG12-B.

of genes such as IL10, IFNγ, TNFα and CXCL9 (Fig. 5E–H) (Oladunni et al., 2020). Taken together, these results further indicate that the genetic differences between SG12-L and SG12-B impacts the clinical outcome of SARS-CoV-2 infection in K18-hACE2 mice.

4. Discussion

Since the emergence of COVID-19, multiple murine infection models involving transduced or transgenic mouse models expressing hACE2 to facilitate SARS-CoV-2 infection have been reported. These include mouse lines altered using permanent genetic modifications such as CAG-hACE2, HFH4-hACE2(Jiang et al., 2020), CRISPR/Cas9 knock-in of hACE2(Sun et al., 2020) or using a mouse adapted SARS-CoV-2 (Dinnon et al., 2020). However, the majority of these models displayed transient weight loss and non-fatal extent of lung injury. While a lethal infection model has been reported, lethality was observed exclusively in animals with detectable brain infection; no lung injury nor weight loss was evident in this HFH4-hACE2 mouse model (Jiang et al., 2020). In addition to the above transgenic models, mice transduced with adenovirus (Ad5-hACE2) or adeno-associated virus expressing hACE2 (AAV-hACE2) have also been shown to be susceptible to SARS-CoV-2 infection, although these animals manifest only mild, non-lethal disease (Israelow et al., 2020). Besides our current report, another group has also reported a lethal K18-hACE2 mouse model(Golden et al., 2020). This group observed considerable weight loss and >90% lethality in SARS-CoV-2 infected mice. However, similar to the HFH4-hACE2 model, lethality was evident in animals that developed a CNS infection.

A drawback of the lethal mouse models thus far is the dominance of CNS pathology as the cause of mortality. Although post mortem analysis of fatal COVID-19 cases have detected SARS-CoV-2 in cortical neurons with immune cell infiltrates suggestive of CNS pathology (Song et al., 2020), with entry to the CNS possibly via the neural-mucosal interface in olfactory mucosa (Meinhardt et al., 2020), the dominant pathology and cause of death in most patients who succumbed to COVID-19 were respiratory dysfunction (Vincent and Taccone, 2020). A mouse model that reliably produces severe and lethal respiratory disease could thus be useful for testing therapeutic and prophylactic strategies against the most common manifestation of severe COVID-19 – acute respiratory distress.

The degree of disease severity observed in this K18-hACE2 model has been attributed to the enhanced levels of hACE2 expression as compared to the other transgenic animal models. The K18 promoter confers efficient transgenic expression of hACE2 in respiratory epithelial cells. However, hACE2 expression has also been observed in the colon, liver, kidney, gastrointestinal tract and brain albeit at low levels of these animals (McCray et al., 2007b). In our study, infection of this transgenic mouse with wildtype SG12 produced both lung and brain infection. Although there was lung pathology similar to what has been observed in fatal COVID-19 cases, the prominent signs that led to euthanasia were mostly attributable to CNS rather than respiratory dysfunction. The

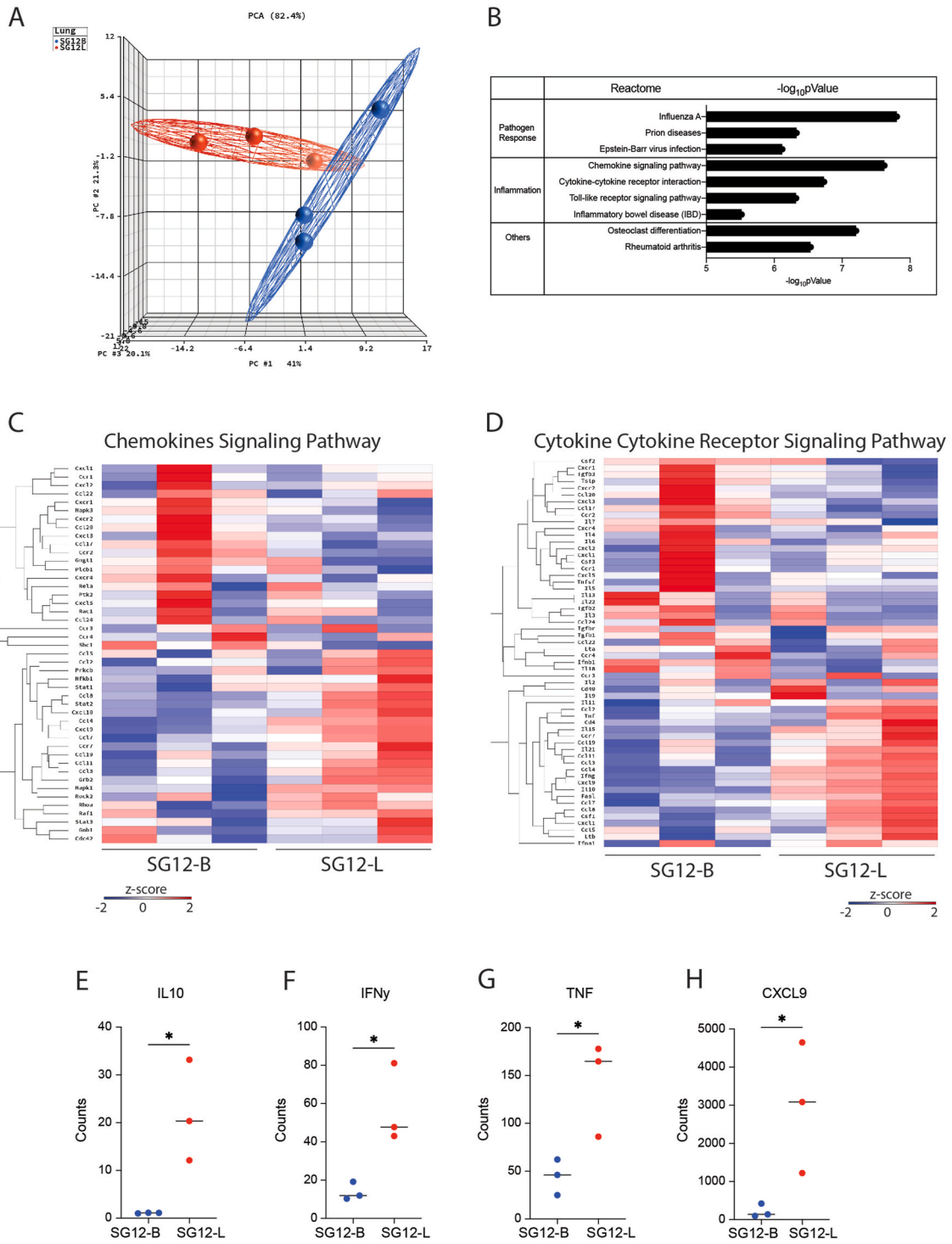

Fig. 5. SG12-L infection in lungs results in increased inflammatory responses.
(A) PCA plot of inflammatory genes of SG12-L (red) and SG12-B (blue) infected lungs. (B) Pathway analysis of the top 20 correlated genes in PC1. (C–D) Heat map showing expression of genes in the chemokine and cytokine-cytokine receptor signaling (E–H) Normalized counts of genes expressed in SG12-B and SD12-L infected K18-hACE2 lungs. (For interpretation of the references to colour in this figure legend, the reader is referred to the Web version of this article.)

distinction in the genomic sequence between SARS-CoV-2 recovered from the lung compared to the brain of the infected animals, as respectively exemplified by SG12-B and SG12-L, thus enabled us to derive viral variants that induce mortality from respiratory rather than CNS dysfunction. These observations were apparent even though infections were performed with non-plaque purified SG12-B and SG12-L once in female mice. However, further studies to elucidate the mechanisms of these mutations should ideally use infectious clone-derived or plaque purified SG12-L and SG12-B viruses. Furthermore, infection in male mice have been reported to have more severe outcomes despite a similar infection rate as compared to female mice (Golden et al., 2020). Investigations on gender-specific response to SG12-L and SG12-B could thus also be informative.

The genome sequence differences between the lung- and brain-

derived SARS-CoV-2 variants also suggest that mutations in the S1–S2 boundary may be important in shaping system-specific pathology. We have focused on attention on high frequency consensus changes only as a limitation of our study is the possibility of false positive nucleotide substitutions among low frequency variants introduced at the PCR tiling step. We identified two high frequency consensus changes C23524T (H655Y) and A23617 (S686G), both residing in the S1–S2 boundary of the S protein, that were present exclusively in the brain isolates. This region contains a polybasic sequence motif - the cleavage site for the host proprotein convertase furin (Örd et al., 2020). Furin mediated cleavage results in S1–S2 to be non-covalently associated for further priming by host serine protease, TMPRSS2, and has been shown to increase the infectivity and tropism of SARS-CoV-2 (Walls et al., 2020a,b). In addition, furin cleavage exposes the C terminus of the S1 protein which has recently been shown to increase internalization of the virus via its CendR sequence binding to NRP1 (Daly et al., 2020). Due to its expression in the olfactory neurons, NRP1 has been found to mediate entry of nanoparticles coated with SARS-CoV-2 derived CendR peptides into the olfactory epithelium, neurons and blood vessels of the cortex (Cantuti-Castelvetri et al., 2020). Taken together, these observations collectively suggest that mutations near or at the S1–S2 cleavage or CendR site may affect infectivity or pathology in the CNS, possibly through spike glycoprotein fusogenicity (Walls et al., 2020a,b). Further studies will be needed to determine how these mutations arise and the mechanism in which mutations in the S1–S2 boundary shape CNS dysfunction.

In conclusion, the identification of SARS-CoV-2 variants that produce lethal pulmonary or CNS infection in K18-hACE2 mice suggest the potential for further development of small animal models for systems level specificity. These models could also serve as resource for testing therapeutic and prophylactic candidates to prevent specific organ dysfunction.

Author contributions

ESG and EEO designed the studies. ESG, BN and SW performed the in vivo experiments. AS performed the viral sequencing. ML and GJS performed the mapping of sequences to protein structures. RR performed the pathological evaluation and interpretation. SZ and THC performed the in vitro experiments. ESG, AS and EEO wrote the manuscript.

Data sharing

Data in this study is available upon request from the corresponding authors at esther.gan@duke-nus.edu.sg or engeong.ooi@duke-nus.edu.sg.

Funding

This study was supported by the National Medical Research Council through the Clinician-Scientist Award (Senior Investigator) to E.E.O.

Declaration of competing interest

The authors declare that they have no known competing financial interests or personal relationships that could have appeared to influence the work reported in this paper.

Acknowledgements

We thank Professor Subhash Vasudevan for facilitating the animal protocols. We acknowledge the Duke-NUS Medical School Biosafety Level 3 facility staff for providing logistic services and care for animals.

Appendix A. Supplementary data

Supplementary data to this article can be found online at https://doi.org/10.1016/j.antiviral.2021.105138.

References

Bao, L., Deng, W., Huang, B., Gao, H., Liu, J., Ren, L., Wei, Q., Yu, P., Xu, Y., Qi, F., Qu, Y., Li, F., Lv, Q., Wang, W., Xue, J., Gong, S., Liu, M., Wang, G., Wang, S., Song, Z., Zhao, L., Liu, P., Zhao, L., Ye, F., Wang, H., Zhou, W., Zhu, N., Zhen, W., Yu, H., Zhang, X., Guo, L., Chen, L., Wang, C., Wang, Y., Wang, X., Xiao, Y., Sun, Q., Liu, H., Zhu, F., Ma, C., Yan, L., Yang, M., Han, J., Xu, W., Tan, W., Peng, X., Jin, Q., Wu, G., Qin, C., 2020. The pathogenicity of SARS-CoV-2 in hACE2 transgenic mice. Nature. https://doi.org/10.1038/s41586-020-2312-y.

Cantuti-Castelvetri, L., Ojha, R., Pedro, L.D., Djannatian, M., Franz, J., Kuivanen, S., van der Meer, F., Kallio, K., Kaya, T., Anastasina, M., Smura, T., Levanov, L., Szirovicza, L., Tobi, A., Kallio-Kokko, H., Österlund, P., Joensuu, M., Meunier, F.A., Butcher, S.J., Winkler, M.S., Mollenhauer, B., Helenius, A., Gokce, O., Teesalu, T., Hepojoki, J., Vapalahti, O., Stadelmann, C., Balistreri, G., Simons, M., 2020. Neuropilin-1 facilitates SARS-CoV-2 cell entry and infectivity. Science, eabd2985. https://doi.org/10.1126/science.abd2985.

Chow, Y.H., O'Brodovich, H., Plumb, J., Wen, Y., Sohn, K.J., Lu, Z., Zhang, F., Lukacs, G. L., Tanswell, A.K., Hui, C.C., Buchwald, M., Hu, J., 1997. Development of an epithelium-specific expression cassette with human DNA regulatory elements for transgene expression in lung airways. Proc. Natl. Acad. Sci. Unit. States Am. 94, 14695–14700. https://doi.org/10.1073/pnas.94.26.14695.

Daly, J.L., Simonetti, B., Klein, K., Chen, K.-E., Williamson, M.K., Antón-Plágaro, C., Shoemark, D.K., Simón-Gracia, L., Bauer, M., Hollandi, R., Greber, U.F., Horvath, P., Sessions, R.B., Helenius, A., Hiscox, J.A., Teesalu, T., Matthews, D.A., Davidson, A. D., Collins, B.M., Cullen, P.J., Yamauchi, Y., 2020. Neuropilin-1 is a host factor for SARS-CoV-2 infection. Science. https://doi.org/10.1126/science.abd3072 eabd3072.

Dinnon, K.H., Leist, S.R., Schäfer, A., Edwards, C.E., Martinez, D.R., Montgomery, S.A., West, A., Yount, B.L., Hou, Y.J., Adams, L.E., Gully, K.L., Brown, A.J., Huang, E., Bryant, M.D., Choong, I.C., Glenn, J.S., Gralinski, L.E., Sheahan, T.P., Baric, R.S., 2020. A mouse-adapted model of SARS-CoV-2 to test COVID-19 countermeasures. Nature 586, 560–566. https://doi.org/10.1038/s41586-020-2708-8.

Golden, J.W., Cline, C.R., Zeng, X., Garrison, A.R., Carey, B.D., Mucker, E.M., White, L.E., Shamblin, J.D., Brocato, R.L., Liu, J., Babka, A.M., Rauch, H.B., Smith, J.M., Hollidge, B.S., Fitzpatrick, C., Badger, C.V., Hooper, J.W., 2020. Human angiotensin-converting enzyme 2 transgenic mice infected with SARS-CoV-2 develop severe and fatal respiratory disease. JCI Insight 5, 507. https://doi.org/10.1172/jci.insight.142032.

Israelow, B., Song, E., Mao, T., Lu, P., Meir, A., Liu, F., Alfajaro, M.M., Wei, J., Dong, H., Homer, R.J., Ring, A., Wilen, C.B., Iwasaki, A., 2020. Mouse model of SARS-CoV-2 reveals inflammatory role of type I interferon signaling. J. Exp. Med. 217, 1033. https://doi.org/10.1084/jem.20201241.

Jiang, R.-D., Liu, M.-Q., Chen, Y., Shan, C., Zhou, Y.-W., Shen, X.-R., Li, Q., Zhang, L., Zhu, Y., Si, H.-R., Wang, Q., Min, J., Wang, X., Zhang, W., Li, B., Zhang, H.-J., Baric, R.S., Zhou, P., Yang, X.-L., Shi, Z.-L., 2020. Pathogenesis of SARS-CoV-2 in transgenic mice expressing human angiotensin-converting enzyme 2. Cell 182, 50–58. https://doi.org/10.1016/j.cell.2020.05.027 e8.

Kaddoura, M., Allbrahim, M., Hijazi, G., Soudani, N., Audi, A., Alkalamouni, H., Haddad, S., Eid, A., Zaraket, H., 2020. COVID-19 therapeutic options under investigation. Front. Pharmacol. 11, 1608. https://doi.org/10.3389/fphar.2020.01196.

Krammer, F., 2020. SARS-CoV-2 vaccines in development. Nature 586, 516–527. https://doi.org/10.1038/s41586-020-2798-3.

McCray, P.B., Pewe, L., Wohlford-Lenane, C., Hickey, M., Manzel, L., Shi, L., Netland, J., Jia, H.P., Halabi, C., Sigmund, C.D., Meyerholz, D.K., Kirby, P., Look, D.C., Perlman, S., 2007a. Lethal infection of K18-hACE2 mice infected with severe acute respiratory syndrome coronavirus. J. Virol. 81, 813–821. https://doi.org/10.1128/JVI.02012-06.

McCray, P.B., Pewe, L., Wohlford-Lenane, C., Hickey, M., Manzel, L., Shi, L., Netland, J., Jia, H.P., Halabi, C., Sigmund, C.D., Meyerholz, D.K., Kirby, P., Look, D.C., Perlman, S., 2007b. Lethal infection of K18-hACE2 mice infected with severe acute respiratory syndrome coronavirus. J. Virol. 81, 813–821. https://doi.org/10.1128/JVI.02012-06.

Meinhardt, J., Radke, J., Dittmayer, C., Franz, J., Thomas, C., Mothes, R., Laue, M., Schneider, J., Brünink, S., Greuel, S., Lehmann, M., Hassan, O., Aschman, T., Schumann, E., Chua, R.L., Conrad, C., Eils, R., Stenzel, W., Windgassen, M., Rößler, L., Goebel, H.-H., Gelderblom, H.R., Martin, H., Nitsche, A., Schulz-Schaeffer, W.J., Hakroush, S., Winkler, M.S., Tampe, B., Scheibe, F., Körtvélyessy, P., Reinhold, D., Siegmund, B., Kühl, A.A., Elezkurtaj, S., Horst, D., Oesterhelweg, L., Tsokos, M., Ingold-Heppner, B., Stadelmann, C., Drosten, C., Corman, V.M., Radbruch, H., Heppner, F.L., 2020. Olfactory transmucosal SARS-CoV-2 invasion as a port of central nervous system entry in individuals with COVID-19. Nat. Neurosci. 395 https://doi.org/10.1038/s41593-020-00758-5, 497–13.

Oladunni, F.S., Park, J.-G., Pino, P.A., Gonzalez, O., Akhter, A., Allué-Guardia, A., Olmo-Fontánez, A., Gautam, S., Garcia-Vilanova, A., Ye, C., Chiem, K., Headley, C., Dwivedi, V., Parodi, L.M., Alfson, K.J., Staples, H.M., Schami, A., Garcia, J.I., Whigham, A., Platt, R.N., Gazi, M., Martinez, J., Chuba, C., Earley, S., Rodriguez, O. H., Mdaki, S.D., Kavelish, K.N., Escalona, R., Hallam, C.R.A., Christie, C., Patterson, J.L., Anderson, T.J.C., Carrion, R., Dick, E.J., Hall-Ursone, S.,

Schlesinger, L.S., Alvarez, X., Kaushal, D., Giavedoni, L.D., Turner, J., Martinez-Sobrido, L., Torrelles, J.B., 2020. Lethality of SARS-CoV-2 infection in K18 human angiotensin-converting enzyme 2 transgenic mice. Nat. Commun. 11, 6122. https://doi.org/10.1038/s41467-020-19891-7.

Örd, M., Faustova, I., Loog, M., 2020. The sequence at Spike S1/S2 site enables cleavage by furin and phospho-regulation in SARS-CoV2 but not in SARS-CoV1 or MERS-CoV. Sci. Rep. 10, 16944 https://doi.org/10.1038/s41598-020-74101-0.

Rockx, B., Kuiken, T., Herfst, S., Bestebroer, T., Lamers, M.M., Oude Munnink, B.B., de Meulder, D., van Amerongen, G., van den Brand, J., Okba, N.M.A., Schipper, D., van Run, P., Leijten, L., Sikkema, R., Verschoor, E., Verstrepen, B., Bogers, W., Langermans, J., Drosten, C., Fentener van Vlissingen, M., Fouchier, R., de Swart, R., Koopmans, M., Haagmans, B.L., 2020. Comparative pathogenesis of COVID-19, MERS, and SARS in a nonhuman primate model. Science 368, 1012–1015. https://doi.org/10.1126/science.abb7314.

Shackelford, C., Long, G., Wolf, J., Okerberg, C., Herbert, R., 2002. Qualitative and quantitative analysis of nonneoplastic lesions in toxicology studies. Toxicol. Pathol. 30, 93–96. https://doi.org/10.1080/01926230252824761.

Song, E., Zhang, C., Israelow, B., Lu-Culligan, A., Prado, A.V., Skriabine, S., Lu, P., Weizman, O.-E., Liu, F., Dai, Y., Szigeti-Buck, K., Yasumoto, Y., Wang, G., Castaldi, C., Heltke, J., Ng, E., Wheeler, J., Alfajaro, M.M., Levavasseur, E., Fontes, B., Ravindra, N.G., Van Dijk, D., Mane, S., Gunel, M., Ring, A., Jaffar Kazmi, S.A., Zhang, K., Wilen, C.B., Horvath, T.L., Plu, I., Haik, S., Thomas, J.-L., Louvi, A., Farhadian, S.F., Huttner, A., Seilhean, D., Renier, N., Bilguvar, K., Iwasaki, A., 2020. Neuroinvasion of SARS-CoV-2 in human and mouse brain. bioRxiv 16, 1169. https://doi.org/10.1101/2020.06.25.169946.

Su, Y.C.F., Anderson, D.E., Young, B.E., Linster, M., Zhu, F., Jayakumar, J., Zhuang, Y., Kalimuddin, S., Low, J.G.H., Tan, C.W., Chia, W.N., Mak, T.M., Octavia, S., Chavatte, J.-M., Lee, R.T.C., Pada, S., Tan, S.Y., Sun, L., Yan, G.Z., Maurer-Stroh, S., Mendenhall, I.H., Leo, Y.-S., Lye, D.C., Wang, L.-F., Smith, G.J.D., 2020. Discovery and genomic characterization of a 382-nucleotide deletion in ORF7b and ORF8 during the early evolution of SARS-CoV-2. mBio 11, 565. https://doi.org/10.1128/mBio.01610-20.

Sun, S.-H., Chen, Q., Gu, H.-J., Yang, G., Wang, Y.-X., Huang, X.-Y., Liu, S.-S., Zhang, N.-N., Li, X.-F., Xiong, R., Guo, Y., Deng, Y.-Q., Huang, W.-J., Liu, Q., Liu, Q.-M., Shen, Y.-L., Zhou, Y., Yang, X., Zhao, T.-Y., Fan, C.-F., Zhou, Y.-S., Qin, C.-F., Wang, Y.-C., 2020. A mouse model of SARS-CoV-2 infection and pathogenesis. Cell Host Microbe. https://doi.org/10.1016/j.chom.2020.05.020.

Vincent, J.-L., Taccone, F.S., 2020. Understanding pathways to death in patients with COVID-19. Lancet Respir Med 8, 430–432. https://doi.org/10.1016/S2213-2600(20)30165-X.

Walls, A.C., Park, Y.-J., Tortorici, M.A., Wall, A., McGuire, A.T., Veesler, D., 2020a. Structure, function, and antigenicity of the SARS-CoV-2 spike glycoprotein. Cell 181, 281–292. https://doi.org/10.1016/j.cell.2020.02.058 e6.

Walls, A.C., Park, Y.J., Tortorici, M.A., Wall, A., Cell, A.M., 2020b. n.d. Structure, Function, and Antigenicity of the SARS-CoV-2 Spike Glycoprotein. Elsevier.

Wan, Y., Shang, J., Graham, R., Baric, R.S., Li, F., Gallagher, T., 2020. Receptor recognition by the novel coronavirus from wuhan: an analysis based on decade-long structural studies of SARS coronavirus. J. Virol. 94, 1986. https://doi.org/10.1128/JVI.00127-20.

Wang, C., Xie, J., Zhao, L., Fei, X., Zhang, H., Tan, Y., Nie, X., Zhou, L., Liu, Z., Ren, Y., Yuan, L., Zhang, Y., Zhang, J., Liang, L., Chen, X., Liu, X., Wang, P., Han, X., Weng, X., Chen, Y., Yu, T., Zhang, X., Cai, J., Chen, R., Shi, Z.-L., Bian, X.-W., 2020a. Alveolar macrophage dysfunction and cytokine storm in the pathogenesis of two severe COVID-19 patients. EBioMedicine 57, 102833. https://doi.org/10.1016/j.ebiom.2020.102833.

Wang, L., Wang, Y., Ye, D., Liu, Q., 2020b. Review of the 2019 novel coronavirus (SARS-CoV-2) based on current evidence. Int. J. Antimicrob. Agents 55, 105948. https://doi.org/10.1016/j.ijantimicag.2020.105948.

Winkler, E.S., Bailey, A.L., Kafai, N.M., Nair, S., McCune, B.T., Yu, J., Fox, J.M., Chen, R. E., Earnest, J.T., Keeler, S.P., Ritter, J.H., Kang, L.-I., Dort, S., Robichaud, A., Head, R., Holtzman, M.J., Diamond, M.S., 2020. SARS-CoV-2 infection of human ACE2-transgenic mice causes severe lung inflammation and impaired function. Nat. Immunol. 21, 1327–1335. https://doi.org/10.1038/s41590-020-0778-2.

Yinda, C.K., Port, J.R., Bushmaker, T., Offei Owusu, I., Purushotham, J.N., Avanzato, V. A., Fischer, R.J., Schulz, J.E., Holbrook, M.G., Hebner, M.J., Rosenke, R., Thomas, T., Marzi, A., Best, S.M., de Wit, E., Shaia, C., van Doremalen, N., Munster, V.J., 2021. K18-hACE2 mice develop respiratory disease resembling severe COVID-19. PLoS Pathog. 17, e1009195 https://doi.org/10.1371/journal.ppat.1009195.

Zhou, F., Yu, T., Du, R., Fan, G., Liu, Y., Liu, Z., Xiang, J., Wang, Y., Song, B., Gu, X., Guan, L., Wei, Y., Li, H., Wu, X., Xu, J., Tu, S., Zhang, Y., Chen, H., Cao, B., 2020. Clinical course and risk factors for mortality of adult inpatients with COVID-19 in Wuhan, China: a retrospective cohort study. Lancet 395, 1054–1062. https://doi.org/10.1016/S0140-6736(20)30566-3.